Chromatin architecture and the orchestration of gene expression: cell systems to explore epigenetic gene control

Brink, M.C.

Publication date
2009

Document Version
Final published version

Chapter 2

MeCP2 revisited: Chromatin Decondensation and the Displacement of HP1γ without Transcriptional Activation

Maartje C. Brink, Diewertje G. E. Piebes, Martijn S. Luijsterburg, Roel van Driel & Pernette J. Verschure

In preparation

Abstract

Methyl-CpG-binding protein 2 (MeCP2) is a chromatin-binding protein involved in the DNA methylation pathway and has been characterized both as a repressor and as a potential activator of transcription. MeCP2 was shown to bind methylated DNA and the epigenetic silencer HP1 and to cause the *in vitro* compaction of chromatin and the *in vivo* formation of repressive chromatin loops. Here we show that, remarkably, the *in vivo* binding of lac repressor-tagged MeCP2 causes extensive decondensation of a lac operator-containing chromosomal domain. The C-terminus of MeCP2 is required for the observed chromatin decondensation, excluding involvement of the methyl-binding and transcriptional-repression domain. MeCP2-induced chromatin decondensation occurs throughout interphase in the absence of changes in CpG methylation. Strikingly, targeted MeCP2 does not activate the transcription of genes embedded in the decondensed chromosomal domain and, in agreement, causes the repression of a luciferase reporter gene *in vivo*. Targeting of MeCP2 triggers the release of HP1γ from the array, but not of HP1α and HP1β. Moreover, over-expression of MeCP2 induces an overall increase of HP1γ mobility. We propose a novel role for MeCP2 in reorganizing chromatin structure in order to facilitate changes in gene expression.

Introduction

The spatial organization of chromatin plays a critical role in the control of eukaryotic gene expression (reviewed by Goetze *et al.*, 2007b). Both the radial positioning of chromatin within the eukaryotic nucleus and folding of the chromatin fiber into more or less condensed states are functionally linked to transcriptional regulation. Establishing the causal relationship between the three-dimensional (3D) chromatin structure and gene activity is an important step towards clarifying the molecular mechanisms underlying eukaryotic gene control. The 3D-chromatin structure is regulated by epigenetic marks, including histone modifications, histone variants and DNA methylation (Chambeyron and Bickmore, 2004; Tumbar *et al.*, 1999). A variety of regulatory proteins are able to specifically bind epigenetic marks and translate these marks to changes in gene expression (Taverna *et al.*, 2007). The interplay between the various epigenetic factors results in an intricate pattern of gene regulation. Previously, we showed that *in vivo* targeting of HP1 to an amplified lac operator-containing chromosomal domain caused local condensation of chromatin structure and recruitment of histone methyltransferase SETDB1, concomitant with methylation of histone 3 at lysine 9 (Verschure *et al.*, 2005). Increasing evidence points towards cross-talk between HP1 and methyl-CpG-binding

proteins. For instance, upon myogenic differentiation the level of methyl-CpG-binding proteins increases, inducing chromocenter clustering concomitant with the relocalization of HP1 to heterochromatin, in particular of the HP1γ isoform (Agarwal *et al.*, 2007; Brero *et al.*, 2005). Additionally, all three HP1 isoforms were found to co-precipitate with methyl-CpG-binding protein 2 (MeCP2; Agarwal *et al.*, 2007).

In the present study, we demonstrate that the *in vivo* targeting of MeCP2 caused extensive chromatin decondensation requiring the C-terminal part of MeCP2. MeCP2-induced chromatin decondensation occurred throughout interphase in the absence of transcriptional activation or changes in CpG methylation. We demonstrate an intricate interplay between MeCP2 and HP1 proteins by showing that MeCP2 promotes eviction of HP1γ from chromatin, but not of HP1α or HP1β. We propose that MeCP2-induced chromatin decondensation reflects a poised status, preparing chromatin for further transcriptional regulation.

Materials and methods

Construction of plasmids

Full-length rat MeCP2 was produced by PCR and cloned into the AscI site of p3'SS-EGFP-dimer lac repressor (Robinett *et al.*, 1996). cDNA of the MeCP2 point mutation R133C (Yusufzai and Wolffe, 2000) was similarly procured. For fusion at the N-terminus of EGFP-lacR, we produced the complete MeCP2 and separate functional domains by PCR, extended with *XbaI* and *XhoI* restriction sites, and cloned these into the identical sites of p3'SS-EGFP-dimer lac repressor. mCherry-lacR and mCherry-lacR-MeCP2 were created by excising EGFP from EGFP-lacR or EGFP-lacR-MeCP2 with *Xba*I and *BsrGI* followed by insertion of mCherry, cut with *NheI* and *BsrGI*.

Cell culture and transfection

The AO3_1 and RRE_B1 cell line are derivatives of CHO DG44, with a condensed or decondensed integration of lac operator repeats and flanking DNA, respectively (Li *et al.*, 1998; Robinett *et al.*, 1996). Cells were regularly cultured in Ham's F-12 without thymidine and hypoxanthine, supplemented with triple dialyzed FBS (Perbio) and 0.1 μM MTX for AO3_1 or 10 μM MTX for RRE_B1 cells, never allowing confluency to reach over 90% or less than 30%. Osteosarcoma cells (U2OS) and NIH/3T3 mouse fibroblasts were cultured in Dulbecco minimal essential medium containing 10% fetal bovine serum. All cells were cultured at 37°C in a 5% CO_2 atmosphere. Cells were transfected at 80% confluency on cover slips coated with Alcian Blue. Alternatively, for live cell experiments, cells were transfected in 35 mm glass bottom dishes (MatTek) at 80% confluency. Transfection was performed with Lipofectamine 2000 according to the manufacturer's protocol. After 24-48 hours, cells were imaged directly or first washed in PBS, fixed in 4% paraformaldehyde for 15 minutes at 4°C and embedded in Vectashield (Brunschwig, Burlingame, CA) with DAPI (4′,6′-diamidino-2-phenylindole; Vector Laboratories, Burlingame, CA). The luciferase reporter gene assay was performed as described elsewhere (Bunker and Kingston, 1996; Verschure *et al.*, 2005).

Immunolabeling and fluorescent *in situ* hybridization

For immunolabeling, cells were permeabilized after fixation with 0.5% (w/v) Triton X-100 in PBS for 5 minutes and incubated in PBS containing 100 mM glycine for 10 minutes. Subsequently, cells were incubated at 4°C overnight with primary antibodies diluted in PBS containing 0.5% (w/v) bovine serum albumin and 0.1% (w/v) gelatin (PBG; Sigma, St. Louis, MO). The following primary antibodies were used:

rabbit anti-H3K9me2 (Upstate, Milton Keynes, United Kingdom; Nakayama *et al.*, 2001), rabbit anti-H3K9me3 (Cowell *et al.*, 2002), rabbit anti-SETDB1 (Schultz *et al.*, 2002), anti-EZH2 and anti-EED (Hamer *et al.*, 2002), rabbit anti-TFIIH p62 subunit (SantaCruz Biotech), mouse anti-SC35 (Abcam; Fu and Maniatis, 1990), mouse anti-histone H1 (Imgen), goat anti-hBrahma (N-19; Santa Cruz Biotechnology), rabbit anti-H3K4me2 (Upstate), rabbit anti-H4K16ac and rabbit anti-H3K27me2 (Upstate). For labeling of DNA methylation, we incorporated a 30-minute denaturation step of 2 M HCl at 37°C and blocked with 10% BSA for 15 minutes, preceding the primary antibody incubation with mouse anti-5mC (Eurogentec) and rabbit anti-lacR, diluted in saline buffer supplemented with 0.5% BSA, 0.1% gelatin and 0.05% tween-20. Primary antibody recognition was achieved by donkey anti-mouse conjugated to biotin and Streptavidin-FITC for anti-5mC and by donkey anti-Rabbit Cy3 for anti-lacR. Fluorescent *in situ* hybridization was performed largely as described elsewhere (Cremer *et al.*, 2001). Denaturation was carried out at 78°C in SSC (0.15 M NaCl, 0.015 M sodium citrate) containing 50% formamide and 10% dextran sulfate. Hybridization was allowed to proceed overnight at 37°C. Posthybridization washes were carried out with 2×SSC/50% formamide at 45°C. All incubations for probe detection were performed at room temperature in 4×SSC containing 5% (w/v) non-fat dried milk.

Run-on transcription labeling

For transcription labeling, BrUTP was incorporated into nascent RNA as described previously (van Royen *et al.*, 2007; Verschure *et al.*, 1999; Wansink *et al.*, 1993). Briefly, cells were permeabilized in glycerol buffer (20 mM Tris HCl, 0.5 mM $MgCl_2$, 0.5 mM EGTA, 25% glycerol and 1 mM PMSF) supplemented with 0.05% Triton X-100, 5 μM DTT and 20 U/ml RNAsin for 3 minutes. BrUTP incorporation was performed for 10 minutes at RT in synthesis buffer (100 mM Tris HCl, 5 mM $MgCl_2$, 0.5 mM EGTA, 200 mM KCl, 50% glycerol, 0.05 mM SAM, 20 U/ml RNAsin, and 0.5 mM PMSF) supplemented with 0.5 mM ATP, CTP, GTP, and BrUTP (Sigma-Aldrich). Cells were fixed and labeled as described above. BrUTP was immunolabeled overnight with rat anti-BrdU (Seralab) diluted 1:500 in PBG at 4°C. Primary antibody detection was followed by biotin-conjugated donkey anti–rat IgG (Jackson ImmunoResearch Laboratories) 1:300 and Cy3-conjugated streptavidin (Jackson ImmunoResearch Laboratories) 1:250.

Image analysis

All cells were imaged using a Zeiss LSM 510 (Zeiss, Jena, Germany) confocal laser scanning microscope equipped with a 63x/1.4 oil immersion objective. We used multitrack scanning, employing a UV laser (364 nm), an argon laser (488 and 514 nm) and a helium neon laser (543 nm) to excite DAPI staining and green and red fluorochromes. Emitted fluorescence was detected with BP 385-470, BP 505-550 and 560 LP filters. Three-dimensional (3D) images were scanned at 512 by 512 pixels using 200 nm axial and 60 nm lateral sampling rates. Images were averaged 4 times. For FLIP and FRAP experiments, microscopes were equipped with an objective heater and cells were examined in microscopy medium (137 mM NaCl, 5.4 mM KCl, 1.8 mM $CaCl_2$, 0.8 mM $MgSO_4$, 20 mM D-glucose and 20 mM HEPES) at 37°C. Surface factor measurements were performed using the Huygens system 2 software package (Scientific Volume Imaging, Hilversum, The Netherlands), as described previously (Verschure *et al.*, 2005). Briefly, the surface factor is calculated as the ratio between the smallest possible surface area of the volume occupied by the array and the actual surface area. A surface factor of 1 therefore represents a perfectly spherical structure, whereas a lower value is assigned to a more furrowed structure. All surface factors were assembled in a histogram (binning 5). The threshold value was set at 0.6, assigning the decondensed chromatin state to all operator arrays with a surface factor lower than 0.6.

Fluorescence Recovery after Photobleaching (FRAP)

FRAP analysis was used to measure the mobility of EGFP-lacR, EGFP-lacR-MeCP2, EGFP-lacR-R133C, C-terminus-EGFP-lacR and MeCP2-EGFP at the lac operator array as described previously (Houtsmuller *et al.*, 1999; Luijsterburg *et al.*, 2007). Briefly, a square of 512x512 pixels was imaged at 2.56 μs per frame, zoom 14 (1 pixel is 0.02x0.02 μm). After 3 images, a strip of 275x150 pixels, encompassing half the lac operator array was bleached by applying 4 scans at maximal 488 and 514 nm laser intensity (AOTF 100%, total time 1.9 s) and the fluorescence recovery was acquired by scanning at least 60 images at a 5-second interval (1x average/frame). For FRAP of EGFP-HP1γ in- and outside of the array, images were taken at 512x512 pixels (0.04x0.04 μm), 1.60 μs per frame, zoom 7. After 10 images, a square of 56x56 pixels was bleached for 10 scans (total time = 1.1 s) and recovery was measured for at least 60 images at a 2-second time interval. The data was normalized to the original intensity before the bleach pulse by using the equation:

$I_{FRAP} = (I_{strip\ t=t} - I_{background\ t=t}) / (I_{strip\ t=0} - I_{background\ t=0})$, where $I_{strip\ t=t}$ and $I_{strip\ t=0}$ represent the intensity within the strip at t=t and the intensity before the bleach pulse (t=0), respectively. For graphical representation, recovery plots were normalized between 0 and 1.

Fluorescence Loss in Photobleaching (FLIP)
FLIP analysis was used to measure the residence time of EGFP-HP1γ on chromatin (Hoogstraten *et al.*, 2002; Luijsterburg *et al.*, 2007). Images of 512x512 pixels were acquired with a scan time of 1.60 µs (1x average/frame) at zoom 7 (1 pixel is 0.04x0.04 µm). After 10 images, a region of 275x150 pixels, occupying an area of 1/3 of the nucleus (excluding the lac operator array), was continuously bleached with maximal 488 nm and 514 nm laser intensity (AOTF 100%). EGFP-HP1γ fluorescence was monitored with low laser intensity for at least 80 images with a 2-second time interval between images. The loss of fluorescence in the unbleached part of the nucleus was quantified. All values were background corrected and normalized to 1 by using the equation: $I_{FLIP} = (I_{spot\ t=t} - I_{background\ t=t}) / (I_{spot\ t=0} - I_{background\ t=0})$. FLIP and FRAP curves were fitted with Igor Pro 5.00 software according to the equation: $y_0 + A_1 \exp(-inv\ Tau_1 x) + A_2 \exp(-inv\ Tau_2 x)$, with $\chi^2 < 0.06$.

Results

MeCP2 fusion proteins localize at mouse chromocenters

To study the effect of MeCP2 binding to chromatin *in vivo*, we fused rat MeCP2 to a fluorescently tagged lacR (EGFP-lacR), enabling targeting and visualization of MeCP2 to an amplified lacO array in living cells (Li *et al.*, 1998). MeCP2 contains a methyl binding domain (MBD), a transcription repression domain (TRD) and a poorly characterized C-terminal domain (Nan *et al.*, 1997; Nan *et al.*, 1993; Nan *et al.*, 1998b). We tagged both full-length MeCP2, as well as the individual domains MBD, TRD, MBD-TRD and the C-terminus of MeCP2, to EGFP-lacR as depicted in figure 1A. In addition, we constructed an EGFP-lacR-tagged version of an MeCP2 point mutation in the MBD domain, R133C, which leads to the development of Rett Syndrome (Ballestar *et al.*, 2000).

MeCP2 naturally resides at heterochromatic sites, such as mouse pericentromeric heterochromatin repeats (chromocenters; Lewis *et al.*, 1992). To demonstrate that our fusion proteins behave similarly to wild-type MeCP2, we assayed their localization in mouse fibroblasts. The MeCP2 domains MBD, MBD-TRD, TRD and point mutant R133C fusion proteins localized to chromocenters similar to full-length MeCP2 (figure 1B-F, H). The EGFP-lacR-tagged C-terminus was homogeneously distributed throughout the nucleus as was the EGFP-lacR control protein (figure 1G and I). The EGFP-lacR-tagged C-terminus lacks the domains associated with methylated DNA and repressor complexes, as found in the MBD, TRD and R133C fusion proteins, and is therefore more likely to display a distribution without enrichment at the chromocenters. These results confirm that all MeCP2-derived fusion proteins except the EGFP-lacR-tagged C-terminus, have a nuclear distribution similar to wild-type MeCP2.

MeCP2 targeting causes local chromatin decondensation

To study the influence of MeCP2 binding on higher-order chromatin structure we targeted the MeCP2-containing lacR fusion proteins in CHO DG44 cell lines containing a highly amplified chromosomal array (of approximately 90 Mb), consisting of tandem lacO repeats interspersed with the DHFR gene. The amplified chromosomal region appeared as either a condensed heterochromatic or an unusually extended fibrillar conformation, in cell line AO3_1 and RRE_B1 respectively (Li *et al.*, 1998; Robinett *et al.*, 1996). Targeting of either N- or C-terminally lacR-tagged MeCP2 induced extensive large-scale decondensation of the amplified chromosomal array in both the AO3_1 and RRE_B1 cell line (figure 2 and data not shown). FISH labeling with a lacO probe confirmed that the fluorescent MeCP2-targeted decondensed structure overlapped completely with the decondensed lacO chromosomal array (figure 3).

The observed decondensation typically occurred in only part (~40%) of the transfected population. To investigate whether MeCP2-induced decondensation is cell-cycle dependent, we transfected AO3_1 cells with EGFP-lacR-MeCP2 and mCherry-tagged proliferating cell nuclear antigen (PCNA). PCNA forms a distinct pattern of replication foci during S-phase and can be used as a marker for cell-cycle stage (Leonhardt *et al.*, 2000). Both condensed and decondensed configurations of the amplified chromosomal arrays upon MeCP2 targeting were observed in cells within S-phase (containing PCNA foci) as well as cells outside of S-phase (not containing PCNA foci; figure 4). Our results show that targeting of EGFP-lacR-MeCP2 results in an extensive decondensation of the amplified chromosomal region in living cells, independent of cell-cycle stage.

The C-terminus of MeCP2 is responsible for chromatin decondensation

To identify the domain of MeCP2 that is essential for the observed decondensation, we targeted individual MeCP2 domains or the Rett-mutant R133C to the amplified chromosomal array in AO3_1 cells. Targeting of lacR-tagged fusion proteins expressing the MBD, the TRD or both these domains, did not clearly decondense the array (figure 5C-E), though occasionally a slightly enlarged array was observed. Conversely, upon targeting of the lacR-tagged C-terminus of MeCP2 or the point mutation R133C, we did observe clear chromatin decondensation, albeit to a lesser extent than full-length MeCP2 (figure 5A, B).

To quantify the degree of decondensation of the array, we collected confocal image stacks of lacO chromatin structures that were the result of targeting full-length MeCP2 proteins or partial MeCP2 domains and measured the extent of decondensation of the chromosomal array, as scored by the parameter 'surface factor' (see materials and methods and de Leeuw *et al.*, 2006; Goetze *et al.*, 2007a; Verschure *et al.*, 2005). The surface factor of ~30 nuclei was plotted in a histogram for each targeted protein,

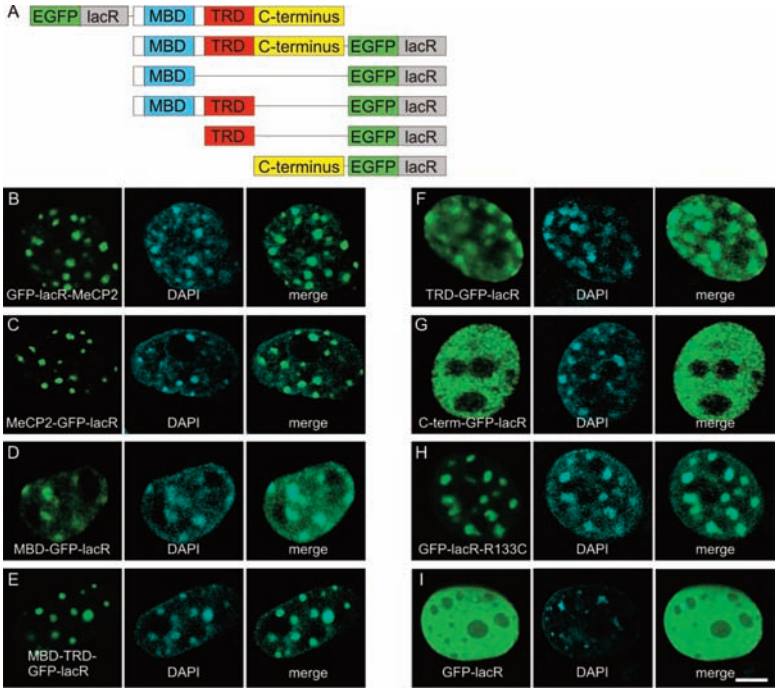

Figure 1. Nuclear distribution of EGFP-lacR-tagged MeCP2 domains in mouse fibroblasts. MeCP2 partial domains were fused in frame to EGFP-lacR and expressed in NIH/3T3 cells. (A) Schematic representation of MeCP2 constructs. (B-I) Cells were fixed, DAPI stained and 3D images were recorded. The images shown represent individual optical sections. The green signal shows the targeting to the chromosomal array of EGFP-lacR-MeCP2 (B), MeCP2-EGFP-lacR (C), MBD-EGFP-lacR (D), MBDTRD-EGFP-lacR (E), TRD-EGFP-lacR (F), C-terminus-EGFP-lacR (G), EGFP-lacR-R133C (H) or EGFP-lacR control (I), the blue signal shows DAPI staining. Nuclei are on the same scale, bar = 5 μm.

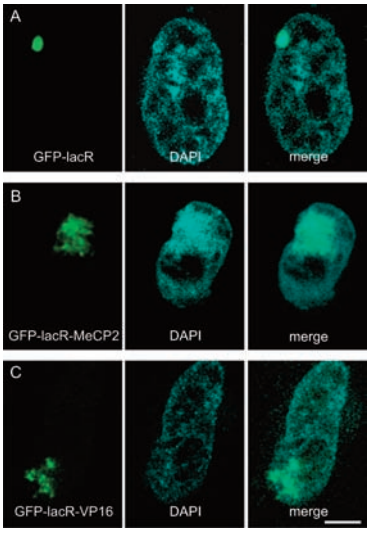

Figure 2. MeCP2 causes chromatin decondensation. AO3_1 cells containing an integrated lac operator domain were transfected with EGFP lacR (control) (A), with EGFP-lacR-MeCP2 (B) or EGFP-lacR-VP16 (C). Cells were fixed, DAPI stained and 3D images were recorded. The green signal shows the targeting of EGFP-lacR with or without full-length MeCP2 at the chromosomal array, the blue signal shows DAPI staining. The images shown represent individual optical sections. Nuclei are on the same scale, bar = 5 μm.

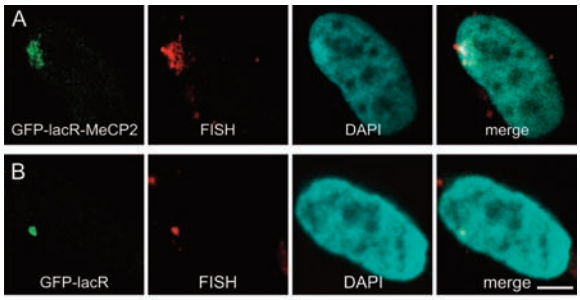

Figure 3. MeCP2-decondensed array contains chromatin. AO3_1 cells were transfected with EGFP-lacR-tagged MeCP2 or the EGFP-lacR control and hybridized with a fluorescently-labeled lac operator DNA probe. Cells were fixed, DAPI stained and 3D images were recorded. The green signal shows the targeting of EGFP-lacR-MeCP2 (A) or of EGFP-lacR (B) to the chromosomal array, the red signal the FISH-labeled lac operator-containing chromosomal array, the blue signal shows DAPI staining. The images shown represent individual optical sections. Bar = 5 μm.

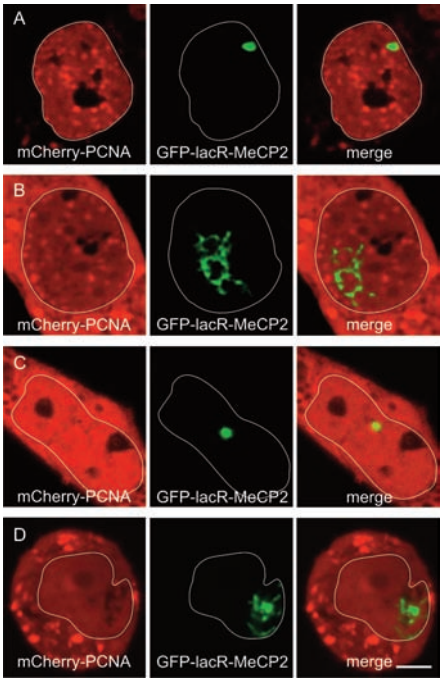

Figure 4. Decondensation is independent of cell-cycle stage. AO3_1 cells were cotransfected with EGFP-lacR-MeCP2 and mCherry-PCNA. Cells were fixed, DAPI stained and 3D images were recorded. The position of the nucleus is indicated by the white line. The green signal shows the targeting of EGFP-lacR-tagged MeCP2 at the chromosomal array, the red signal shows mCherry-PCNA. The images shown represent individual optical sections. Nuclei are on the same scale, bar = 5 μm.

displaying a bimodal distribution that reflects cell nuclei containing either a condensed or a decondensed chromosomal array. The ratio of the two distributions provides information on what fraction of cells contains decondensed arrays. Figure 5F depicts the percentage of nuclei containing decondensed arrays for all targeted proteins. Compared to the decondensation induced by lacR-MeCP2 according to the surface factor, lacR-tagged VP16, MeCP2 (N-terminal), C-terminus and R133C were not significantly different (one-tailed Mann Whitney test, $P<0.05$), causing similar levels of decondensation. In contrast the lacR control and lacR-tagged MBD, TRD and MBDTRD did not cause decondensation and were significantly different to lacR-MeCP2. These quantitative results mirrored our visual observations: the degree of decondensation of the chromosomal array was most pronounced in the cells targeted by fusion proteins containing an intact C-terminus of MeCP2. We conclude that the C-terminal domain of MeCP2 plays a pivotal role in MeCP2-induced chromatin decondensation.

Untargeted MeCP2 causes decondensation of the amplified chromosomal array

To determine whether decondensation of the MeCP2-targeted chromosomal array was a result of fusion of MeCP2 to the lacR, we expressed fluorescent MeCP2 without a lacR tag in AO3_1 cells. Untargeted MeCP2-mRFP (*i.e.* not fused to the lacR) localized at the amplified lacO array, both in EGFP-lacR control and in EGFP-lacR-MeCP2 transfected cells (Figure 6A, B). Furthermore, MeCP2-mRFP caused decondensation at the amplified array in the lacR-expressing cells, albeit to a lesser extent than in the lacR-targeted MeCP2 cells. To consolidate our microscopic observations, we quantified the extent of decondensation in MeCP2-mRFP-expressing cells by measuring the surface factor of the chromosomal array. In the MeCP2-mRFP-expressing cells the surface factor differs significantly from that in lacR-targeted control cells ($P<0.01$), however decondensation induced by untargeted MeCP2 also differs significantly from the extensive decondensation induced by targeted lacR-MeCP2. The percentage of cells with a decondensed array is shown in figure 5F. Untargeted MeCP2 decondenses the amplified lacO chromatin to a much smaller extent than lacR-targeted MeCP2 both in volume of the array (as measured by the surface factor) and in percentage of cells in which the effect is observed (figures 2B, 5F and 6A). We considered the possibility that differences in residence times between untargeted MeCP2 and lacR-targeted MeCP2 were responsible for causing different degrees of chromatin decondensation. In order to determine residence times of untargeted and targeted MeCP2, we performed FRAP (Fluorescence Recovery After Photobleaching) analysis. Bleaching was performed on a region covering one third of the lacO array followed by monitoring fluorescence recovery of the various EGFP-tagged proteins. Figure 6C shows that in control cells, EGFP-lacR was nearly fully immobilized at the amplified lacO array: we detected almost no recovery of fluorescence after the bleach pulse during the detection period. In cells expressing lacR-MeCP2, the immobilization of the lacR-tagged MeCP2 was even more pronounced. Similar results were obtained for lacR-tagged R133C and lacR-tagged C-terminus (data not shown). In contrast, untargeted MeCP2 was mobile at the amplified lacO array with a $t_{1/2}$ of ~24s (mono-exponential fit). These results illustrate that lacR-fused MeCP2 or partial MeCP2 domains are tightly bound to the array by the lacR-lacO interactions and do not exchange on a time-scale of minutes in contrast to MeCP2 without a lacR-tag. It is tempting to speculate that the residence time of molecules bound at the array, influenced by differences in affinity and available binding sites, determines the degree of chromatin decondensation.

MeCP2 induces the displacement of HP1γ

A potential interaction between MeCP2 and the HP1 proteins was recently identified by co-immunoprecipitation of MeCP2 and HP1γ from mouse cells (Agarwal *et al.*, 2007). Co-transfections of mCherry-lacR-tagged MeCP2 and EGFP-tagged HP1α, HP1β or HP1γ in AO3_1 cells showed that the three HP1 isoforms are enriched at the

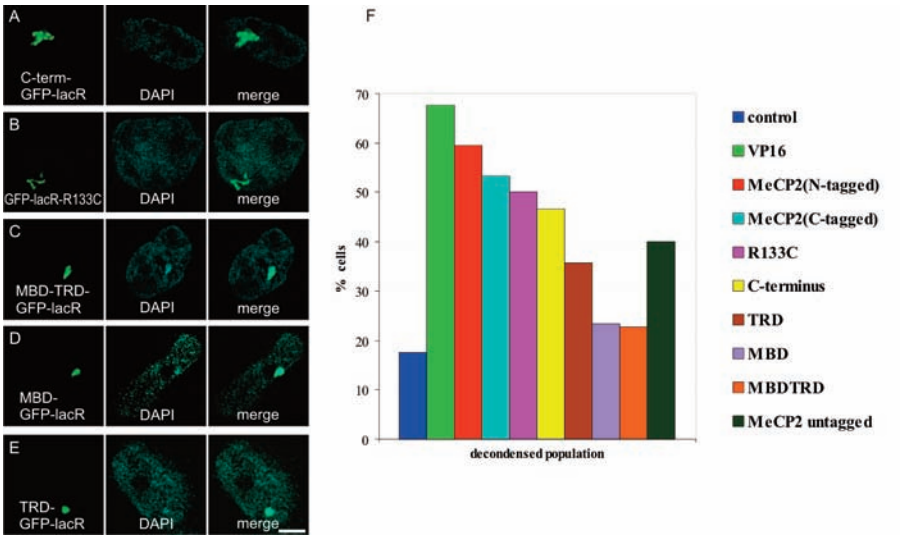

Figure 5. The MeCP2 C-terminal domain is responsible for chromatin decondensation. MeCP2 partial domains were fused to EGFP-lacR and expressed in AO3_1 cells. Cells were fixed, DAPI-stained and imaged in 3D. Image analysis software identified the array within each nucleus and calculated the corresponding surface factors. Targeting of the EGFP-lacR-tagged C-terminal domain (A), R133C (B), MBDTRD (C), MBD (D) and TRD (E) at the amplified array. The green signal shows the targeting of EGFP-lacR or EGFP-lacR-tagged MeCP2 domains at the chromosomal array, the blue signal shows DAPI staining. The images shown represent individual optical sections. Nuclei in panels A-E are on the same scale. Bar = 5 μm. (F) Plotting of the surface factor distributions revealed the fraction of the amplified arrays in condensed state. The histogram shows the percentage of cells that have a decondensed array upon targeting by all EGFP-lacR-tagged proteins and upon expression of untagged MeCP2.

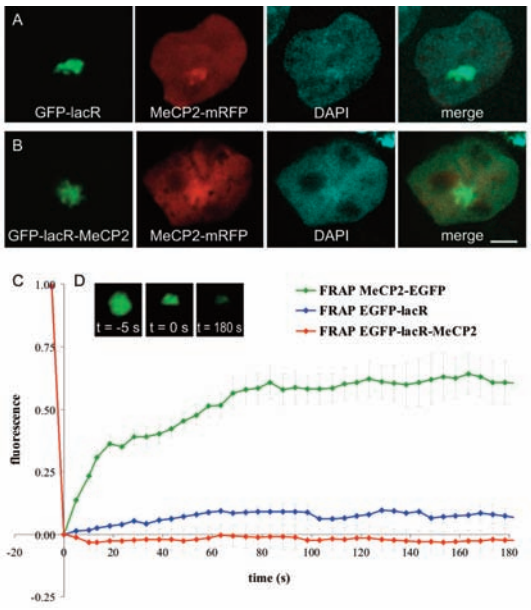

Figure 6. Untargeted MeCP2 localizes to and decondenses the lac operator array. AO3_1 cells were co-transfected with MeCP2-mRFP and either EGFP-lacR or EGFP-lacR-MeCP2. A bleach pulse was administered, bleaching half of the lac operator array. Subsequent fluorescence recovery was measured during 3 minutes. 3D-projection of transfected AO3_1 nucleus co-transfected with untargeted MeCP2-mRFP and EGFP-lacR (A) or optical section of AO3_1 nucleus co-transfected with MeCP2-mRFP and EGFP-lacR-MeCP2 (B). The green signal shows the targeting of EGFP-lacR or EGFP-lacR-tagged full-length MeCP2 at the chromosomal array, the red signal shows the expressed MeCP2-mRFP. Bar = 5 μm. (C) FRAP curves of untargeted MeCP2-EGFP, control EGFP-lacR and EGFP-lacR-MeCP2 fusion proteins. Inset (D) shows the lac-operator array targeted by EGFP-lacR before, immediately after and 3 minutes after the bleach pulse.

chromosomal array (visualized by the mCherry-lacR protein) in the absence of MeCP2 targeting (figure 7A, C and E). Strikingly, HP1γ accumulation at the amplified array was lost after targeting lacR-tagged MeCP2, both at the condensed and the decondensed arrays (figure 7B and data not shown). Conversely, HP1α and β remained bound after MeCP2 targeting (figure 7D, F). These results show that targeting of MeCP2 interferes with the binding of HP1γ at the amplified array, but not with that of HP1α and HP1β.

To quantify the effect of MeCP2 on HP1γ binding to the amplified array, we determined HP1γ mobility using FRAP. A small square of the nucleus of an EGFP-HP1γ-transfected cell was bleached either in- or outside of the amplified region, visualized by mCherry-lacR, and subsequent fluorescent recovery was measured (figure 7G). Fitting of the two FRAP curves identified two HP1γ populations of different mobility both in- and outside of the array. Outside of the amplified array, the largest fraction (~90%) of the HP1γ population displayed fast mobility ($t_{1/2}$ = 1.4 s), likely representing freely diffusing HP1γ. Approximately 10% of the protein pool displayed slower exchange and was considered chromatin-bound HP1γ ($t_{1/2}$ = 12.0 s). Measurements in the amplified domain revealed a marked shift in the distribution of the freely diffusing versus chromatin-bound HP1γ populations. At the amplified array only 57% of the HP1γ population displayed high mobility whereas 43% of the protein pool showed reduced mobility, indicating efficient accumulation of HP1γ at the amplified array in the absence of MeCP2 targeting.

Next, we performed FLIP (Fluorescence Loss In Photobleaching) of HP1γ in the presence of lacR or lacR-MeCP2, by continuously bleaching part of the nucleus outside of the amplified domain and performing simultaneous measurements on the loss of fluorescence in the rest of the nucleus (figure 7H). Fitting of the FLIP curves identified two HP1γ pools; one highly mobile, freely diffusing population and a less mobile, bound population. The lacR-transfected control cells displayed free diffusion for 71% of the HP1γ proteins ($t_{1/2}$ = 3.1 s). Strikingly, the proportion of the freely diffusing HP1γ population went up to 97% ($t_{1/2}$ = 1.5 s) after targeting of lacR-tagged MeCP2. Moreover, in the presence of untargeted MeCP2, we measured an increase in unbound HP1γ (94%), similar to that in lacR-MeCP2 transfected cells. These results confirm that MeCP2 effectively antagonizes direct or indirect binding of HP1γ to chromatin.

Localization of MeCP2-associated factors upon MeCP2 targeting

Apart from the eviction of HP1γ upon MeCP2 targeting, we were unable to detect local accumulation or displacement of several tested factors (see table 1 and materials and methods). We did not detect the activating factors CREB1 or TFIIB that were shown to interact with MeCP2 (Chahrour *et al.*, 2008; Kaludov and Wolffe, 2000). Other factors and epigenetic marks associated with transcription (RNAPII, H3K4 dimethylation and H4K16 acetylation), were not enhanced after MeCP2 binding. The chromatin-remodeling complex SWI/SNF has been suggested to interact *in vivo* with

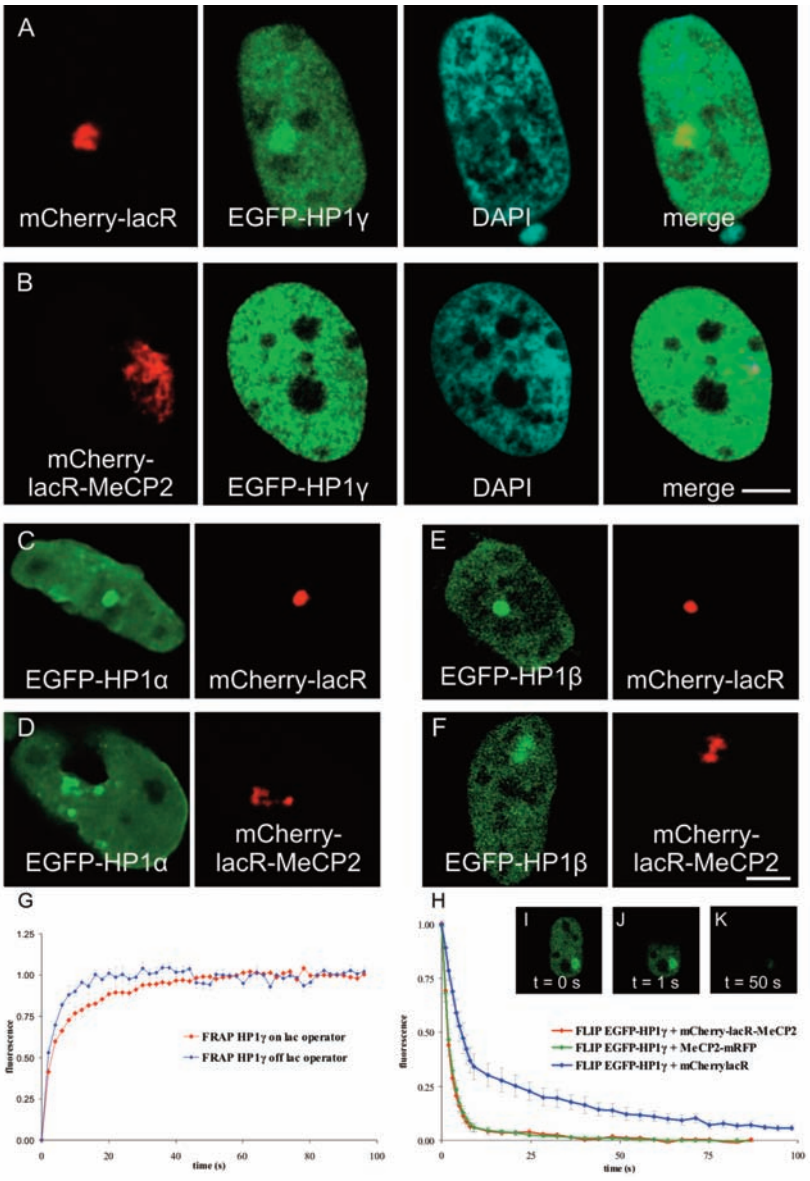

Figure 7. MeCP2 interferes with HP1γ binding. Optical sections of AO3_1 nucleus transfected with mCherry-lacR and HP1γ (A), HP1α (C) or HP1β (E) or mCherry-lacR-MeCP2 and HP1γ (B), HP1α (D) or HP1β (F). The red signal shows the targeting of mCherry-lacR or mCherry-lacR-MeCP2 at the chromosomal array, the green signal shows the expressed EGFP-tagged HP1 isoforms. Nuclei in A-B and in C-F are on the same scale. Bars are 5 μm. (G) FRAP curve of HP1γ in- and outside of the array. (H) FLIP curves of HP1γ in the presence of mCherry-lacR-MeCP2, MeCP2-mRFP or mCherry-lacR. The insets (I-K) show an EGFP-HP1γ and mCherry-lacR-expressing cell of which half of the nucleus is continuously bleached (only green channel is shown). FLIP was measured in the unbleached half of the nucleus.

Table 1. Localization of MeCP2-associated factors at the amplified array with and without EGFP-lacR-MeCP2 targeting. Various factors were assayed for their presence at the amplified lacO-containing array by immunolabeling or co-transfection, upon either EGFP-lacR (control) or EGFP-lacR-MeCP2 targeting. Localization at the array is indicated by: (+) present, (+/-) sometimes present or (-) absent.

labeling	**control**	**MeCP2**
H3K9me2	+/-	+/-
H3K9me3	+/-	+/-
H1	+/-	+/-
EZH2	+/-	+/-
EED	-	-
p62 (TFIIH)	-	-
hBrahma	-	-
H3K4me2	-	-
H4K16ac	-	-
H3K27me2	-	-
SC35	-	-
SETDB1	-	-
mCpG	+	+
transfection	**control**	**MeCP2**
H1	+/-	+/-
RNAPII	-	-
TFIIH	-	-
CREB	-	-
Dnmt1	-	-
Dnmt3b	-	-
HP1α	+	+
HP1β	+	+
HP1γ	+	-

MeCP2 through its catalytic subunit Brahma, though other reports did not detect such an interaction (Harikrishnan *et al.*, 2005; Hu *et al.*, 2006; Wang, 2003). We did not detect enhanced accumulation of Brahma after MeCP2 targeting. Additionally, MeCP2 has been shown to compete with histone H1 for chromatin binding sites (Nan *et al.*, 1997; Nikitina *et al.*, 2007a). Eviction of H1 from chromatin by MeCP2 could explain changes in chromatin structure, however we did not observe any changes in H1 distribution upon MeCP2 targeting. The C-terminus of MeCP2 is able to bind RNA splicing factors (Buschdorf and Stratling, 2004). We considered the possibility that lacR-MeCP2 relocalizes chromatin to SC35 domains or speckles, nuclear bodies enriched in mRNA splicing factors (Lamond and Spector, 2003). Antibody labeling of SC35 identified no co-localization between SC35 domains and the MeCP2-decondensed chromatin array. MeCP2 was originally described as a protein that binds to methylated DNA (Lewis *et al.*, 1992). Therefore, we examined DNA methylation levels at the amplified chromosomal array in those cells showing extensive decondensation of the array upon lacR-MeCP2 targeting. We visualized the *in situ* DNA methylation levels using 5-methylcytosine immunolabeling, which allows analysis at the single-cell level. Methylated CpGs were concentrated at the amplified array both in lacR-MeCP2-targeted and in lacR-targeted control cells (figure 8A and B), illustrating that the observed chromatin decondensation is not related to a change in DNA methylation.

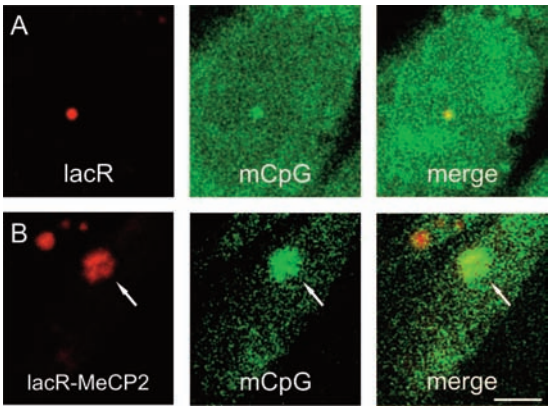

Figure 8. DNA methylation. AO3_1 cells were transfected with mCherry-lacR (A) or mCherry-lacR-MeCP2 (B) and immunolabeled for the presence of lacR and methylated CpGs after denaturation. Cells were fixed, DAPI stained and 3D images were recorded. The red signal shows labeling of mCherry-lacR or mCherry-lacR-tagged MeCP2 at the chromosomal array, the green signal shows 5-methyl-cytosine labeling. Arrows indicate the array. The images shown represent individual optical sections. Nuclei are on the same scale. Bar = 5 µm.

Targeted MeCP2 maintains transcriptional repression *in vivo*

Wild-type MeCP2 acts as a transcriptional repressor, both *in vitro* and *in vivo* (Nan *et al.*, 1997; Nan *et al.*, 1998a). To confirm that MeCP2 maintains its repressive characteristics upon decondensing the amplified chromosomal domain, we performed BrUTP labeling of nascent RNA. This approach allows us to identify changes in the amount of transcripts originating from the chromosomal array in individual cells that display decondensation upon MeCP2 targeting. BrUTP incorporation into newly synthesized RNA was performed on AO3_1 cells transfected with lacR-MeCP2 or with the lacR control. We observed no visible increase of BrUTP-labeled transcript levels at the decondensed amplified chromosomal array upon MeCP2 targeting compared to

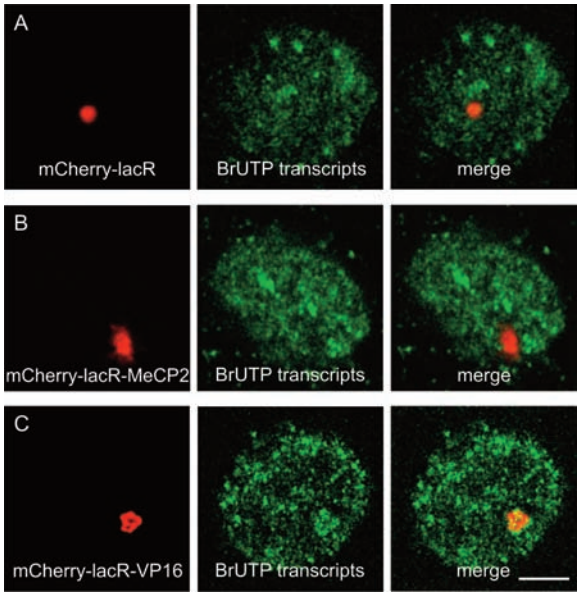

Figure 9. MeCP2 maintains transcriptional silencing at the decondensed lac operator array. AO3_1 cells were transfected with mCherry-lacR (A), mCherry-lacR-MeCP2 (B) or mCherry-lacR-VP16 (C). Cells were permeabilized and incubated with BrUTP for 10 minutes, fixed and stained by immunolabeling. 3D images were recorded. The red signal shows the targeting of mCherry-lacR or mCherry-lacR-tagged MeCP2 or VP16 at the chromosomal array, the green signal shows the nascent RNA. The images shown represent individual optical sections. Nuclei are on the same scale. Bar = 5 µm.

transcript levels at the array in lacR-targeted cells (figure 9A and B). We did observe a considerable increase in BrUTP-labeled transcripts at the chromosomal domain after targeting lacR-VP16, correlated with chromatin decondensation (figure 9C and shown previously by Tumbar *et al.*, 1999). To prove that targeted MeCP2 and other constructs used in this study repress gene expression, we measured the gene expression levels of a luciferase reporter gene fused to 8 lacO copies, upon lacR targeting of MeCP2 (Verschure *et al.*, 2005). The reporter construct was transiently expressed in U2OS cells, together with lacR-tagged MeCP2, R133C or partial MeCP2 domains. MeCP2, R133C and the MBDTRD domain of MeCP2 significantly inhibited luciferase expression compared to the lacR control (60-70%). Interestingly, in contrast to the other MeCP2-derived fusion proteins, the tagged C-terminus only caused repression to a moderate extent (~10%). Taken together, these results demonstrate that the lacR-tagged MeCP2 protein is able to repress gene activity of a transiently expressed luciferase reporter gene. We show that decondensation of the amplified chromosomal array upon MeCP2 targeting does not correlate with gene activation.

Discussion

Regulation of mammalian gene expression is a tightly controlled process. Mistakes in the orchestration of the thousands of genes can have far-reaching consequences, such as the manifestation of various developmental disorders or cancer. For example, mutations in the epigenetic regulator MeCP2 cause the developmental disorder known as Rett Syndrome (Amir *et al.*, 1999). Yet, it remains unclear how MeCP2, a protein embedded in the DNA methylation pathway, influences epigenetic regulation. In previous studies we have shown that targeting of silencing proteins, such as HP1, to an amplified chromosomal array condenses higher-order chromatin structure (Brink *et al.*, 2006; Verschure *et al.*, 2005). These findings are in agreement with the general notion that silencing proteins associate with condensed chromatin.

Here, we provide evidence that the relationship between gene activity and spatial chromatin organization is not straightforward. We show that targeting of MeCP2 to a lacO-containing amplified chromosomal domain induces decondensation of this heterochromatic structure without gene activation. We present evidence that the C-terminus of MeCP2 mediates the observed chromatin decondensation and that MeCP2-induced chromatin decondensation is correlated with the release of bound HP1γ, but not of HP1α and of HP1β.

MeCP2 decondenses chromatin *in vivo*

We demonstrate that the C-terminal domain of MeCP2 is capable of decondensing chromatin, excluding involvement of the MBD and TRD in restructuring chromatin. In previous *in vitro* studies, the C-terminal domain of MeCP2 was shown to bind chromatin and suggested to play a role in restructuring chromatin architecture by

inducing, contrary to our observations, chromatin compaction (Georgel *et al.*, 2003; Nikitina *et al.*, 2007b). However, *in vitro* reconstituted nucleosomal arrays lack higher-order chromatin structure that is present in the interphase nucleus of living cells, probably invoking a different response to the binding of MeCP2. The observed MeCP2-induced *in vivo* chromatin decondensation suggests that polymer cross-linking is not a major activity of MeCP2 in living cells. In mouse myoblasts, over-expression of MeCP2 resulted in chromatin compaction by the clustering of chromocenters during myogenic differentiation, an effect dependent on the MBD of MeCP2 (Brero *et al.*, 2005), whereas in this study chromatin decondensation is achieved by the C-terminal MeCP2 domain. An explanation for the discrepancy between our data and the findings by Brero and colleagues likely relates to the type of chromatin investigated (mouse chromocenters contain specialized repetitive DNA, such as *Alu* and satellite repeats) and the type of MeCP2 domain that is involved, *i.e.* the MBD or the C-terminal domain.

Chromatin restructuring by MeCP2 is independent of transcriptional activation
We show that transcription remains repressed after targeting of MeCP2, despite the fact that the amplified chromatin domain is extensively decondensed, similar to the decondensed chromatin structure induced by targeting the viral activator VP16 (Tumbar *et al.*, 1999). Accordingly, we found no evidence for the presence of activating factors CREB1 or TFIIB that have been previously associated with MeCP2 (Chahrour *et al.*, 2008; Kaludov and Wolffe, 2000). Also RNAPII and epigenetic marks associated with transcriptional competence, *i.e.* H3K4 dimethylation and H4K16 acetylation, were not enhanced upon MeCP2 targeting, confirming that MeCP2-induced decondensation occurs independent of transcription. These observations illustrate a deviation from the canonical model in which condensed chromatin is considered silent and decondensed chromatin is considered active. In concordance with our findings, analysis of the transcriptional activity of sucrose-gradient-isolated chromatin fibers revealed that both transcriptionally active and inactive sites occur in compact as well as in less compact chromatin fibers (Gilbert *et al.*, 2004).

Similar to the epigenetic silencer HP1 which binds to both active and inactive chromatin according to ChIP and DamID (de Wit *et al.*, 2007; Vakoc *et al.*, 2005), MeCP2 has been found associated with both active and inactive neuronal promoters (Yasui *et al.*, 2007). One report argued that MeCP2 can switch the gene expression state to either repression or activation (Chahrour *et al.*, 2008). In light of such a proposed function for MeCP2, the opening up of chromatin by MeCP2 observed in this study could reflect an indeterminate state in which the targeted locus is poised for transcription. Examples of changes in chromatin structure preceding a transcriptional activation have been reported previously for the HoxB and MHC locus (Chambeyron and Bickmore, 2004; Volpi *et al.*, 2000). We propose that by unfolding chromatin structure, MeCP2 switches chromatin from a transcriptionally restrictive to a permissive state. In this scenario, the recruitment of additional activating or repressive factors subsequently decides the transcriptional fate of genes embedded within the permissive chromatin.

MeCP2 and DNA methylation

Several studies hint at a relationship between DNA methylation levels, the presence of methyl-CpG-binding proteins and changes in chromatin structure. In the absence of DNA methylation in mouse embryonic stem cells lacking Dnmt3a and 3b, a genome-wide increase in H3K9me3 and histone acetylation as well as chromocenter clustering is observed (Gilbert *et al.*, 2007). On the other hand, during myogenic differentiation, over-expression of methyl-CpG-binding proteins induced increased DNA methylation levels and chromocenter clustering, independent of the H3K9 histone methylation pathway and requiring the MBD domain of MeCP2 (Brero *et al.*, 2005). Our data do not implicate a role for DNA methylation in the MeCP2-induced chromatin restructuring, which is not surprising considering that the C-terminal domain and not the MBD of MeCP2 is the prominent domain involved in decondensation. These findings demonstrate that the causal relationship between MeCP2, DNA methylation levels and changes in chromatin structure are still unclear.

Eviction of HP1γ upon MeCP2 binding

Interestingly, we find that MeCP2 inhibits HP1γ binding at the chromosomal array. Our FRAP analysis shows that HP1γ is retained at the array in the absence of MeCP2 targeting, possibly due to the heterochromatic nature of the amplified array. Indeed, we measure similar kinetics of HP1γ at the array as previously measured at heterochromatic sites in mouse cells (Cheutin *et al.*, 2003; Schmiedeberg *et al.*, 2004). Surprisingly, MeCP2 binding triggers the release of HP1γ, reflected by the loss of local HP1γ accumulation at the amplified array after MeCP2 targeting and by the globally altered HP1γ mobility upon MeCP2 over-expression. Strikingly, HP1α and β, which are essential for HP1γ recruitment to heterochromatic sites, are still present at the amplified domain (Dialynas *et al.*, 2007). Possibly, MeCP2 inhibits HP1γ binding by steric hindrance or by structurally changing the substrate through chromatin decondensation. Displacement of HP1γ was previously observed preceding transcriptional activation at a luciferase reporter gene integrated in breast cancer cells (Vicent *et al.*, 2008). Here, a hormonal signaling cascade leads to phosphorylation of H3S10, displacement of HP1γ and subsequent ATP-dependent chromatin remodeling, providing an open chromatin structure as 'landing platform' for the transcription machinery (Vicent *et al.*, 2008). It is tempting to speculate that the eviction of HP1γ and decondensation of the chromosomal array after MeCP2 binding are part of a mechanism to prepare chromatin for transcriptional changes.

Our results show that MeCP2 is an architectural protein that has the ability to unfold condensed chromatin, while maintaining transcriptional silencing. We propose that MeCP2 is a versatile protein that affects higher-order chromatin structure in order to prepare genomic domains for changes in gene expression.

Acknowledgements

We thank Wim de Leeuw for help on the operation of the Huygens software, Suzanne Kooistra for performing the luciferase reporter assay measurements and Federico Tessadori for critical reading of the manuscript. Plasmids MeCP2-mRFP and MeCP2-EGFP were received from C. Cardoso (Berlin, Germany), EGFP-HP1 plasmids from P. Hemmerich (Jena, Germany; Schmiedeberg *et al.*, 2004), EGFP-TFIIB from Danyang Chen (Sui Huang Lab, Chicago, USA), EGFP-RNAPII from W. Vermeulen (Rotterdam, the Netherlands), EGFP-CREB1 from H. Eldar-Finkelman (Tel Aviv, Israel), mCherry-PCNA from C. Dinant (Rotterdam, the Netherlands; Dinant *et al.*, 2007) and EGFP-H1 from N.P. Dantuma (Karolinska Institutet, Stockholm). This work was supported by the Netherlands Organisation for Scientific Research (NWO, project number VIDI2003/03921/ALW/016.041.311).